IEEE Robotics and Automation Letters (RA-L) paper, presented at ICRA 2024, Yokohama, Japan. Cite as RA-L paper.

Magnetic Field-Driven Bristle-Bots

Lukáš Supik[1,2], Kateřina Stránská[1], Miroslav Kulich[1], Libor Přeučil[1], Michael Somr[3], and Karel Košnar[1]

***Abstract*—Widespread demand for mobile robots is pushing the research envelope for the development of new robot driving mechanisms that can handle diverse environments. Bristle-bot-like robot designs, investigated increasingly over the past decade, are based on vibration mechanisms built on flexible legs that enable motion on the ground. However, creating scalable and steerable bristle-bots remains a challenge. Therefore, we developed a new kind of magnetic field-driven bristle-bots with a wireless control and power supply that can be steered and downscaled. Therefore, in our experimental study with a working prototype, we developed a new kind of magnetic field-driven bristle-bot designed for wireless control and power supply. These bristle-bots can thus be steered and downscaled.**

We verified our concept experimentally using 3D-printed bristle-bots with body-embedded permanent magnets actuated via torque imposed by an external magnetic field. An AC-powered Helmholtz coil generated the bristle-bot's driving field, providing 2D input control, field amplitude, and frequency. A variable number of legs on each side of a bristle-bot's body was used to ensure that each side of these sides has a different frequency response. This asymmetry introduced steerability with a rich set of control commands, including rotations with simultaneous forward and backward locomotion. We also observed side locomotion not yet described in previous studies. The results presented were supported with data from numerous experiments and thorough statistical analysis, indicating promising directions for future bristle-bot development.

***Index Terms*—Bristle-Bots; Magnetic Actuation, Friction Interactions, Wireless Power Supply, Motion Control**

I. INTRODUCTION

MOBILE robots are becoming a part of everyday life, with applications ranging from autonomous vacuum cleaners to delivery robots to autonomous cars. The success of these applications has increased the demand for new robot features and capacities. This paper discusses three main trends influencing mobile robot innovation. The first, downscaling, requires reducing complexity while preserving locomotion capabilities. Second, there is a demand for mobile robots to be deployed in various environments. Third, there are calls for making such robots more affordable for mass production and use. Robot swarms, where thousands of units operate, represent one example, necessitating simplicity and low unit costs.

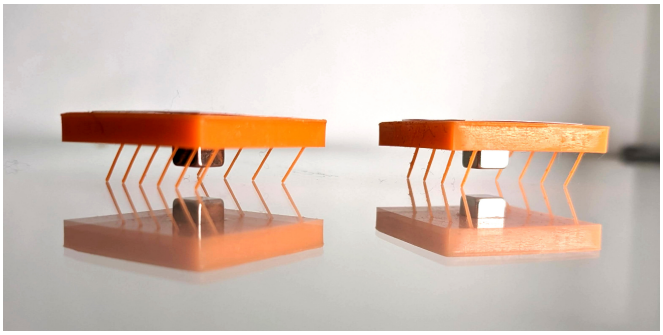

Fig. 1: 3D printed bristle-bots placed on glass. Embedded neodymium magnets in an external magnetic field are the receivers of the control inputs and driving power.

Two types of robots have been designed to address such demands: worm-like robots and bristle-bots. Worm-like robots have flexible bodies covered by flexible legs. Gradual contractions and extensions of their bodies result in a translation of the entire robot [1], [2], [3]. Bristle-bots have rigid bodies embedded with actuators that stand on inclined, flexible legs. This type of robot is a simple mechanical oscillator that moves because the leg tips periodically switch from stick to slip phases on the ground. The advantage of bristle-bots over worm-like robots is that they can be scaled down [4], [5], [6] and used in special environments. Possible applications include pipeline inspections and rescue systems [7]. Furthermore, their simple design facilitates low-cost manufacturing and opens up many possibilities for massive applications in swarms [8], [9]. Finally, Jílek et al. [10] have proposed using bristle-bots in macro-scale self-assembly, which can be seen as a macroscopic simulator of thermodynamic phenomena (crystalization, DNA synthesis, among others), and this work makes the first step towards the experimental validation of the proposed concepts.

The legs and the bodies of bristle-bots form mechanical oscillators actuated by the vertical force from a mechanical vibrator [11], [7], [12], [13] or piezo-electrical actuator [5], [14], [4]. Since the legs are inclined, they can be modeled with rotational springs and thus can convert vertical oscillations to horizontal ones because of the friction between the legs and the ground. While increasing actuation amplitude, horizontal inertial forces overcome static friction, and the tips of the legs start moving back and forth in a horizontal direction. Surprisingly, the friction may be different for forward and backward motion, influencing overall locomotion of a robot's body. Cicconofri and de Simone [15] provided an analytical

Manuscript received DD.MM.2023; accepted DD.MM.2023. Date of publication DD.MM.2023; date of current version DD.MM.2023. This paper was recommended for publication by Editor Clement Gosselin upon evaluation of the Associate Editor and Reviewers' comments.

[1]Lukáš Supik, Kateřina Stránská, Miroslav Kulich, and Libor Přeučil are with the Czech Institute of Informatics, Robotics and Cybernetics, IMR Department, Czech Technical University in Prague, Prague 16636, Czech Republic (email: lukas.supik@cvut.cz)

[2]Lukáš Supik is with the Department of Cybernetics, Faculty of Electrical Engineering, Czech Technical University in Prague, Prague 12135, Czech Republic

[3]Michael Somr is with the Faculty of Civil Engineering, Czech Technical University in Prague, Prague 16636, Czech Republic.

Digital Object Identifier (DOI): see top of this page.

IEEE Robotics and Automation Letters (RA-L) paper, presented at ICRA 2024, Yokohama, Japan. Cite as RA-L paper.

IEEE Robotics and Automation Letters (RA-L) paper, presented at ICRA 2024, Yokohama, Japan. Cite as RA-L paper.

model for the bristle-bot motion that explained the role of the actuation frequency and the bot's eigenfrequency. In particular, actuation at lower frequencies than the eigenfrequency leads to higher normal forces at the leg tips for forward motion than for backward motion. Hence, backward motion is preferred, since it needs to overcome a lower friction force than forward motion. Actuation in frequencies higher than eigenfrequency has the opposite effect, and actuation at eigenfrequency causes a robot to slide in the same place. Consequently, the velocity and direction of a bristle-bot can be controlled through actuation frequency. Despite the fact that Cicconofri and de Simone [15] assumed an atypical force model, subsequent works assuming the Coulomb friction model provided quantitatively-consistent results [14].

Since bristle-bot designs can be simple, the manufacture of such inexpensive robots that could be miniaturized while maintaining steerability (which appears to correlate with a robot's dimensions) seems promising. Trade-offs between complexity and steering capabilities have been investigated. Becker et al. [7], in their pioneering work, examined bristle-bots actuated by excentric flywheels driven by electric motors, with $60\times40\times35$ mm^3 bristle-bots having a maximum velocity of 200 mm$\cdot$s^{-1}. However, these bristle-bots were only able to move forward, and their relatively high velocity was probably caused by an entire robot jumping. Notomista et al. [13] and Majewski et al. [12] came up with complex bristle-bots driven by two or three independent excentric flywheels driven by electrical motors. These complex bristle-bots could move forward and turn left and right, but no backward motion was observed. Majewski et al. [12] manufactured 50×80 mm^2 bristle-bots on a rectangular platform and achieved a maximum velocity of 66 mm$\cdot$s^{-1}.

Another strand of research focuses on bristle-bots with simple designs capable of motion inversion. Cicconofri et al. [16] examined $55\times35\times9$ mm^3 bristle-bots and observed forward motion of 2.5 mm$\cdot$s^{-1} and backward motion of 1.2 mm$\cdot$s^{-1}. Similarly, Kim et al. [14] examined $10\times8\times5$ mm^3 bristle-bots observed with 30 mm$\cdot$s^{-1} forward motion and 10 mm$\cdot$s^{-1} backward motion.

Others have focused on microscopic bristle-bots with simple designs; however, motion inversion had not yet been observed. Kim et al. [5] examined 5 mg bristle-bots with a characteristic 1 mm size, observing forward movement at a velocity of 8 mm$\cdot$s^{-1}. Moreover, Kim et al. [6] examined $233\times113\times75$ μm^3 magnetic bristle-bots that reached a velocity of 5 μm$\cdot$s^{-1}.

Significant success in overcoming the trade-offs between complexity and steering capabilities was achieved by Hao et al. [4]. Their piezo-electrically-actuated $12\times8\times6$ mm^3 bristle-bots were designed asymmetrically with different leg thicknesses (consequently, different eigenfrequencies) on each side. Actuation at the proper frequency activated left, right, or both sides. Hao et al. [4] observed 37 mm$\cdot$s^{-1} forward motion and backward motion with a velocity of 2 mm$\cdot$s^{-1}. However, during streering, side locomotions (63 mm$\cdot$s^{-1} and of 32 mm$\cdot$s^{-1} velocities) appeared instead of circular trajectories. A natural explanation for this unexpected result is the undesirable influence of the wires powering the actuator.

Contributions

Despite the recent advances in the field, the remaining challenge in developing scalable and steerable bristle-bots is improving actuation and the power supply mechanism while preserving scalability and steerability. Hao et al. [4] designed simple, steerable bristle-bots. However, their wired power system affected their motion, negatively influencing measurements, and limiting downscaling. To date, only one study has examined promising actuation and power supply mechanisms to overcome limitations related to wired power. Kim et al. [6] produced micro-scale bristle-bots covered by a nickel layer magnetized in an external magnetic field. As a result of magnetization, these bristle-bots experienced torque and moved due to the oscillations in an alternating magnetic field. This successful stable motion by micro-scale bristle-bots was observed only for forward movement, however.

In our study, inspired by Kim et al. [6], we designed magnetic actuation with permanent magnets instead of a magnetized layer. Second, inspired by Hao et al. [4], we implemented asymmetric design controllability modified for a torque actuation scenario. In contrast to Kim et al. [6], our bristle-bots exhibited forward and backward motion for their left and right legs, implying controllability. In contrast to Hao et al. [4], our wireless power system makes scalability of the bristle-bots as well as measurement of left- and right-side leg motion possible without unwanted external force. As a result, we observed a shift between resonant characteristics for both sides, supporting the concept of the controllability of asymmetric design as proposed by Hao et al. [4]. Moreover, the shape of measured resonant characteristics corresponded to the theoretical predictions made by Cicconofri and de Simone [15]. This study's novel contributions are that:

- We elaborated on a *novel actuation principle*: torque actuation.
- We tuned the bristle-bot's *steerable design* controlling the motion of the left and right sides separately. (Fig. 3).
- We demonstrated our concepts on a *working prototype* with a scalable[1] and steerable bristle-bot (Fig. 1). We identified actuation frequencies for various driving modes, enabling us to control driving modes. The driving modes included clockwise (CW) and counter-clockwise (CCW) rotations plus forward and side translations. Importantly, side translation is a new phenomenon not yet described in previous bristle-bot studies.
- We conducted a *statistical analysis* of experiments we performed enabling us to observe the effects of printing and measurement errors on bristle-bot motion, showing that despite printing errors, all printouts had similar motion trends and were controllable.

This paper is structured as follows. Section II provides a theoretical analysis of magnetic actuation and experimental

[1]The limits of downscaling are of particular interest. Regarding 3D printing, two-photon polymerization was used for microscale bristle-bots manufacturing [5], [6] and its resolution is the hundreds of nanometers (Faraji et al. [17]). Therefore, bristle-bots could be scaled down up to tens of micrometers. Regarding permanent magnets, the minimum size of nanoparticles with ferromagnetic behavior is given by superparamagnetism and is also tens of micrometers (Reichel et al. [18]).

IEEE Robotics and Automation Letters (RA-L) paper, presented at ICRA 2024, Yokohama, Japan. Cite as RA-L paper.

IEEE Robotics and Automation Letters (RA-L) paper, presented at ICRA 2024, Yokohama, Japan. Cite as RA-L paper.

Fig. 2: Bristle-bot in Helmholtz coil, which generated a homogeneous vertical magnetic field. The upper coil ring was placed above the workspace, and the lower coil ring was placed under the workspace (only partially visible).

results and provides motion equations. Section III describes magnetic actuation, mechanical properties, and motion detection for our bristle-bots, with Section IV providing magnetic actuation properties and steerable capabilities. Section V summarizes our experimental results and outlines possibilities for further research.

II. Theoretical Principles

A. Magnetic Field in Helmholtz Coil

For actuation of our magnetic bristle-bots, a Helmholtz coil was used because it generates an approximately homogeneous magnetic field that enables the calculation of forces and torque that act on a permanent magnet. In our design, the magnetic field amplitude was not directly measured, and hence it was calculated from the electric current supplied in the coil.

A Helmholtz coil consists of two coil rings, each with radius R, placed in parallel at distance R. Each coil ring has n turns and is supplied by current I. The magnitude of magnetic induction $|\mathbf{B}|$ at the center of the Helmholtz coil can be expressed as [19]

$$|\mathbf{B}| = \left(\frac{4}{5}\right)^{3/2} \frac{\mu_0 n I}{R} \tag{1}$$

where μ_0 is the permeability of free space. The magnetic field heads along the axis of the Helmholtz coil.

To maximize the space where bristle-bots could move in a nearly homogeneous field, we oriented the axis of the Helmholtz coil vertically and let the bristle-bots move in a horizontal plane placed symmetrically between coil rings (Fig. 2). The quantitative description of the field inhomogeneities was provided by Bronaugh [20]. In our experiments, the bristle-bots could move maximally $0.6R$ away from the coil center, corresponding to a 10% decrease in the field intensity (Fig. 2 in reference [20]).

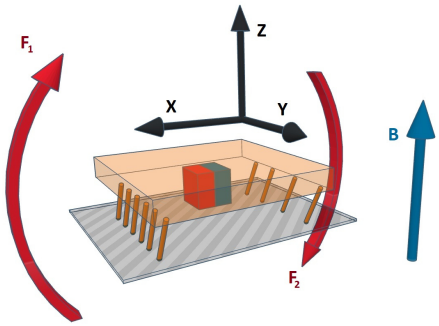

Fig. 3: Bristle-bot design with embedded permanent magnet and asymmetric number of legs on both sides. The black arrows define the local coordinate system, the blue arrow shows the orientation of magnetic induction, and the red arrows show the force couple acting on the permanent magnet.

B. Bristle-Bots Mechanics

Since the magnetic field of the Helmholtz coil is close to homogeneous, it is reasonable to assume that the permanent magnet embedded in the bristle-bot's body can be fully described by its magnetic moment $\mathbf{m}$. The force $\mathbf{F}_m$ and torque $\boldsymbol{\tau}_m$ acting on a permanent magnet in a homogeneous magnetic field can be expressed as [21]

$$\mathbf{F}_m = \mathbf{0}, \tag{2}$$

$$\boldsymbol{\tau}_m = \mathbf{m} \times \mathbf{B}. \tag{3}$$

Regarding interaction of a bristle-bot's legs with the ground, the forces from all legs were summed up to total force $\mathbf{F}_l$ and torque $\boldsymbol{\tau}_l$. Therefore the equations of motion of the bristle-bot's body can be expressed as

$$\frac{d\mathbf{p}}{dt} = \mathbf{F}_l + \mathbf{F}_g \tag{4}$$

$$\frac{d\mathbf{L}}{dt} = \boldsymbol{\tau}_m + \boldsymbol{\tau}_l \tag{5}$$

where $\mathbf{p}$ and $\mathbf{L}$ stand for momentum and angular momentum respectively. $\mathbf{F}_g$ denotes gravitational force. We state the equations of motion without further analysis, since this is beyond the scope of this paper; however, we would like to analyze these in greater depth in our future work[2].

C. Analysis of Bristle-Bots Motion

Due to the challenging nature of the measuring complete 3D bristle-bot motion, we only analyzed planar motion. Therefore, the velocity of a bristle-bot can be expressed as $\mathbf{v} = (v_x, v_y, 0)$ and angular velocity as $\boldsymbol{\omega} = (0, 0, \omega)$ in its reference frame (Fig. 3), with v_y representing forward velocity and v_x side velocity.

Moreover, we decomposed translation $\mathbf{v}$ and rotation $\boldsymbol{\omega}$ to the forward (in direction of y-axis) velocities of the left legs

[2]Further details regarding equations of motion (appropriate formalism, their derivation, and solving approaches), can be found in classical mechanics textbooks such as Goldstein's *Classical Mechanics* [22]. Concretely, the most relevant chapters are generally those discussing kinematics and the dynamics of a rigid body.

IEEE Robotics and Automation Letters (RA-L) paper, presented at ICRA 2024, Yokohama, Japan. Cite as RA-L paper.

TABLE I: Helmholtz Coil Parameters

Parameter	Value	Parameter	Value
radius R	31.5 cm	number of turns n	200 [1]
inductance	46 mH	wire cross-section	1.5 mm^2

[1] Each of the two coil rings had 200 turns

TABLE II: Bristle-Bot Mechanical Properties

Parameter	Value	Parameter	Value
leg length	6.5 mm	Young modulus	1.2 GPa
leg diameter	0.5 mm	block dimensions	2.5×2.5×3 mm^3
leg inclination	60°	mass	3.7 g

v_l and the forward velocity of right legs v_r. Including side locomotion, which was the same for both sides v_s, the mapping from the motion of bristle-bots to the motion of legs can be expressed as

$$\begin{pmatrix} v_l \\ v_r \\ v_s \end{pmatrix} = \begin{pmatrix} 0 & 1 & -\frac{d}{2} \\ 0 & 1 & \frac{d}{2} \\ 1 & 0 & 0 \end{pmatrix} \begin{pmatrix} v_x \\ v_y \\ \omega \end{pmatrix} \tag{6}$$

where d is the distance between the left and right legs; note that the transformation matrix in equation 6 is full rank; hence, both descriptions contain the same information.

Finally, we report resonant characteristics, which are velocities as functions of actuation frequency. In particular, we report resonant characteristics of the left and right sides, v_l and v_r, since these illustrate the effects of asymmetric design. According to Cicconofri and de Simone [15], zero of resonant characteristic corresponds to bristle-bot natural frequency (for the case of symmetric design). Therefore, we report zeros of resonant characteristics of left and right sides as natural frequencies of corresponding sides[3].

D. Statistical Inference

The uncertainty of bristle-bot motion in our study was classified into two groups. First, the 3D printer used to manufacture the bristle-bots had limited precision; hence, each printed bot had different mechanical properties and velocities at external actuation. Second, repeated measurements of the same printout led to different bot velocities. This can be explained mainly because of different initial conditions, including the position and orientation of a robot. The velocity varied because the paper testing surface was not perfectly homogeneous and could be slightly inclined. Finally, the Helmholtz coil magnetic field was not perfectly homogeneous, as discussed in subsection II-A.

In this regard, let us model a random process for general scalar velocity y_{ij} of printout i at measurement j. Therefore, i ranges from 1 to p, and j ranges from 1 to n, where p and n stand for the numbers of printouts and repetitions of each measurement respectively. Note that in this study, we take $p = n = 10$, and y represents one of the velocities $\{v_l, v_r, v_s\}$. The adopted model takes the form:

$$y_{ij} = \mu_i + \nu_{ij} \tag{7}$$

where we assume that μ_i are independent random draws from a distribution $\mathcal{D}(\mu, \sigma_\mu^2)$ with mean μ and variance σ_μ^2 and ν_{ij} are random draws from a distribution $\mathcal{D}(0, \sigma_\nu^2)$ with zero mean and variance σ_ν^2. Regarding the interpretation of distribution parameters, μ stands for the velocity of an ideally-printed bristle-bot under ideal measurement conditions while σ_μ and σ_ν are standard 3D printing and measurement errors, respectively. The unbiased sample estimators of the introduced parameters are

$$\hat{\mu}_i = \frac{1}{n}\sum_{j=1}^{n} y_{ij}, \tag{8}$$

$$\hat{\sigma}_{\nu i}^2 = \frac{1}{n-1}\sum_{j=1}^{n} (y_{ij} - \hat{\mu}_i)^2, \tag{9}$$

$$\hat{\mu} = \frac{1}{p}\sum_{i=1}^{p} \hat{\mu}_i, \tag{10}$$

$$\hat{\sigma}_\nu^2 = \frac{1}{p}\sum_{i=1}^{p} \hat{\sigma}_{\nu i}^2, \tag{11}$$

$$\hat{\sigma}_\mu^2 = \frac{1}{p-1}\sum_{i=1}^{p} (\hat{\mu}_i - \hat{\mu})^2 - \frac{1}{n}\hat{\sigma}_\nu^2. \tag{12}$$

The estimators μ_i and $\hat{\sigma}_{\nu i}^2$ are the mean and sample variance over different measurements for each printout i. The estimators $\hat{\mu}$ and $\hat{\sigma}_\nu^2$ are the averages over different bristle-bots printouts. Finally, $\hat{\sigma}_\mu^2$ is the variance estimator for 3D printing consisting of a "standard" variance estimator corrected for bias.

Note that the presented estimators are scalar; however, the velocity of a bristle-bot is a 3D vector. Although it is possible to estimate velocity as a vector with corresponding covariance matrices instead of scalar variances, the number of measurements would be insufficient for making this kind of estimation. In the 1D case, there are 100 measurements for estimating 3 parameters (μ, σ_μ, and σ_ν). For a 3D case, there are 300 measurements for estimating 21 parameters (3 for expected velocity, and 9 for both 3×3 covariance matrices).

III. Experimental Design

A. Properties of Helmholtz Coil and Permanent Magnets

Table I provides the parameters of the Helmholtz coil used in this study. The coil was supplied by amplified harmonic signals from a function generator. We chose harmonic actuation since this is typical for mechanical oscillators. Since the maximum output voltage of the amplifier was 30 V and Helmholtz coil inductance was 46 mH, the frequency limit to obtain a reasonable coil current of 1.25 A was 120 Hz. It is possible to calculate the magnitude of magnetic induction $|\mathbf{B}|$ using electric current I with Eq. 1. For particular values of coil parameters, the current-to-field ratio was $|\mathbf{B}|[\mathrm{mT}] = 1.1\, I[\mathrm{A}]$.

[3]The idea of asymmetric design, proposed by Hao et al. [4], assumes that the left and right sides behave approximately as independent oscillators. In this approximation, it is reasonable to report zeros of resonant characteristics of the left and right sides as natural frequencies of both sides. Nevertheless, the natural frequencies of our bristle-bots may differ, and their derivation would require solving the equations of motion Eqs. 4 and 5.

IEEE Robotics and Automation Letters (RA-L) paper, presented at ICRA 2024, Yokohama, Japan. Cite as RA-L paper.

The torque $\boldsymbol{\tau}_m$ acting on the bristle-bot in the magnetic field can be calculated using Eq. 3 from a known magnetic dipole moment m. Therefore, the magnetic dipole moment was measured in the experiment by examining the force acting on a dipole in a stationary magnetic field. The resulting value was $|\mathbf{m}| = 0.145\ \mathrm{A} \cdot \mathrm{m}^2$.

B. Bristle-Bot Design, Manufacturing, and Mechanical Properties

Each bristle-bot was made from a square plate with inclined legs on two parallel yz-planes (Fig. 3) inclined 60° to the horizontal xy-plane. The bristle-bots were manufactured on a 3D resin printer and Table II provides their mechanical properties. The bristle-bots had four legs on the left and six on the right. This particular proportion was chosen based on the preliminary experiments, where bristle-bots with various leg ratios were tested. (The selection criterion was the number of characteristic driving modes.)

C. Detecting Bristle-Bot Motion

To enable efficient tracking of a robot's position during experiments, we relied on an AprilTags [23] visual tracker. A regular camera suspended above the workspace observes the visual tags placed on the robots. This setup allowed us to segment and track the tags used and thus provided position and heading of the bristle-bots, thus allowing computation of their velocities.

IV. Results

This work's main contribution is an innovative design and elaboration of a novel driving principle for magnetic bristle-bots. Regarding driving principles, various driving modes were expected based on previous theoretical research; however, it was uncertain that the principles used in force-based actuation can be applied for torque actuation scenarios. Therefore, identifying different driving modes for torque-actuated bristle-bots supports existing theories describing bristle-bot motion. Moreover, discovering unexpected driving modes, particularly side locomotion, challenges current models and suggests further theoretical analysis is needed.

The motion of bristle-bots was measured in one comprehensive and automatized experiment, as seen in Supplementary Video 1. First, an external mechanism moved a bristle-bot to the center of the Helmholtz coil, if it was in a marginal region. Second, a coil driving current from $\{0.5,\ 0.75,\ 1,\ 1.25\}$ A and a frequency f ranging from 10 to 104 Hz were selected. Third, the coil was supplied with electric current for 2 seconds and bristle-bot motion was detected. Overall, the experiment consisted of 13,600 submeasurments for 4 amplitudes, 34 frequencies, 10 printouts, and 10 repetitions.

In the following subsections, results from the same experiment are presented. However, different frequency subsets and driving currents, together with different quantities, were selected and presented. In the subsection IV-A, the trajectories at frequencies $\{32,\ 40,\ 44,\ 52,\ 60,\ 64\}$ Hz and coil driving current of 1 A are presented. Moreover, two specific driving modes (32 and 52 Hz) are analyzed in detail, focusing on the consequences of the variation among bristle-bot printouts. This exemplifies the effects of both error types: printing and measurement errors. In subsection IV-B, bristle-bot behavior in terms of velocities as the response to external actuation is presented for the whole dataset. Finally, subsection IV-C presents bristle-bot frequency response in terms of velocities of left- and right legs for 1 A coil driving current. This representation let us understand bristle-bot behavior and enabled comparison with previous studies. Printing and measurement errors were also visualized.

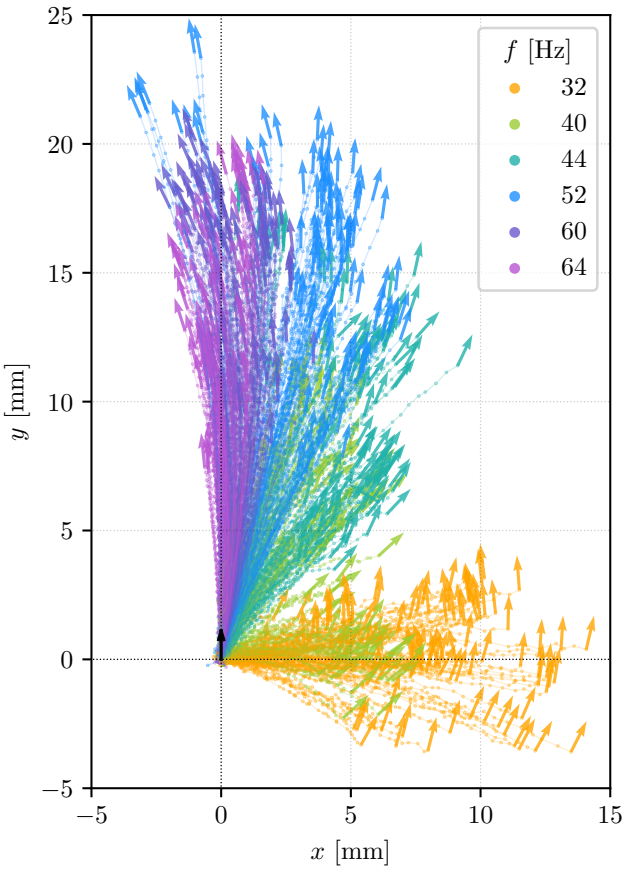

Fig. 4: Trajectories of different bristle-bot printouts at various frequencies with 2 second measurements. The origin of the coordinate system is the initial position of a bristle-bot (black arrow) and the final bristle-bot positions are denoted by colored arrows. The bristle-bots started with side locomotion to the right at 32 Hz with statistically insignificant rotations. At 44 Hz, the bristle-bots moved forward with CW rotation. At 52 Hz, a mode of forward locomotion with negligible rotation started. The highest frequencies used were for forward locomotion and CCW rotations (60 and 64 Hz).

A. Trajectories of Characteristic Driving Modes

The trajectories of the selected modes are shown in Fig. 4. There is a notable transition from side locomotion at lower frequencies to forward locomotion at higher frequencies. Moving to the differences among the printouts of bristle-bots

IEEE Robotics and Automation Letters (RA-L) paper, presented at ICRA 2024, Yokohama, Japan. Cite as RA-L paper.

caused by printing errors, Fig. 5 shows the separate trajectories of bristle-bots at 32 and 52 Hz. The colors of the trajectories indicate individual bristle-bot printouts, and it is clear that printing-induced deviations had a greater effect on motion than measurement errors. The relatively low measurement errors highlight the reproducibility and controllability[4] of bristle-bot motion. Comparing our results to Hao et al. [4], the trajectories were not affected by powering wires, and thus exhibited arc shapes according to predictions.

B. Control Map

This section describes the response of the bristle-bots to actuation at different frequencies and amplitudes in terms of velocities and angular velocities. We call this response the "control map" and it appears in Fig. 6. The control map summarizes all sub-measurements and both types of velocities are averages over measurement repetitions and different bristle-bot printouts. However, velocity errors are not visualized here.

For practical purposes, the resulting bristle-bot motions were composed of translation and rotation; hence, both quantities had to be considered simultaneously. For example, at 44 Hz and 1 A, a bristle-bot moved forward with CW rotation, resulting in a trajectory curved to the right (Fig. 4 provides a comparison). Moreover, at 24 Hz and 1 A, there was a CCW rotation with negligible translation; at 36 Hz and 1 A, there was a CW rotation with negligible translation. Therefore, the bristle-bots could turn right and left on the spot. The driving modes observed imply that bristle-bots can be controlled[5] over a rich set of various trajectories, demonstrated in Supplementary Video 2. In comparison to other studies, our control map is unique since it provides the mapping from the frequency-amplitude domain to the velocities of the entire planar motion (v_x, v_y, ω).

C. Resonant Characteristic of Asymmetric Bristle-Bots

The control map was therefore helpful for control and steering of bristle-bots in the experimental workspace. However, understanding motion patterns by analyzing the control map itself is complex. Therefore, bristle-bot translation and rotation are decomposed to the velocity of left legs v_l, the velocity of right legs v_r, and their side locomotion v_s according to Eq. 6. The resonant characteristics for 1 A of coil driving current are shown in Fig. 7. Two-level areas envelop the resonant curves. The richer color describes measurement standard errors, and the paler color describes printing standard errors defined by Eqs. 11 and 12. The following patterns can be observed from Fig. 7.

[4]The word "controllability" is used in a loose sense and it does not correspond exactly to the definition used in control theory. In this paper, "controllability" refers to a bristle-bot's ability to reach arbitrary configuration in its state space, e.g., x, y position and heading θ.

[5]Here, we intentionally describe the ability to follow various trajectories instead of general ones. The reason is that proper analysis of a bristle-bot's controllability in the system control framework is beyond the scope of this study. Moreover, the supplementary video does not present the motion controlled by the standard controller. We decided to control bristle-bots manually using a laptop keyboard. (The laptop set generator frequency based on keyboard input.)

First, resonant characteristics for both sides started with statistically significant backward locomotion, which continuously transitioned to forward locomotion at higher frequencies. The pattern is similar to theoretical results from Cicconofri and de Simone [15]. Second, the right side had more legs (6) than the left side (4), which resulted in a higher right-side stiffness and natural frequency. Hence, the right-side resonant characteristic was shifted to frequencies higher than the left-side resonant characteristic. Third, the side locomotion resonant characteristic seemed to have two resonant peaks. Comparing our results to experimental studies examining milli-bristle-bots ([4] and [14]), our resonant curves were non-zero in a wide range of frequencies, in contrast to the sharp resonant peaks described in previous studies. However, we observed sharp resonant peaks in measurements with low actuation amplitudes. Therefore, our results are consistent with Hao et al. [4] and Kim et al. [14].

V. Conclusions

This work introduced a novel concept for creating magnetically driven bristle-bots manufactured and examined experimentally. Using the torque actuation principle instead of force actuation, we achieved wireless power supply and control. This, along with the bristle-bot's simple design, show promise for future downscaling of such robots, which could eventually lead to the development of passive micro-robots. Our bristle-bots, while simple in their design, exhibited several different motion modes and thus followed various trajectories. The current limitations of our concept lie in a certain randomness of motion. This is due to uncontrolled factors in our study, notably the inherent inaccuracy of our 3D printing process and measurement errors. However, thanks to a thorough statistical analysis, we were able not only to distinguish but also to quantitatively identify the source of these errors.

Regarding future research directions, we would like to focus on more general actuation signals generating on-demand commands. In particular, asymmetric signals present an attractive option for motion based on switching between stick and slip phases. Strong and short impulses can lead to a slip phase, whereas weak and long impulses can lead to a stick phase, resulting in overall motion. Furthermore, it would be desirable to calculate optimal control input based on a mechanical bristle-bot model. Another promising research area is the design and control of a multi-robot system. Generally, more heterogeneous responses to external signals mean individual robots can be controlled more easily in such a system. In addition to differences in mechanical design, asymmetric signals would allow bristle-bots to be distinguished from each other according to the orientation of the magnetic dipole moments embedded in their bodies.

Finally, we believe that the proposed design of magnetically-actuated bristle-bots is rather universal and opens the way to interesting and innovative future applications. In particular, the bristle-bots could be used in macroscopic thermodynamic simulators or swarm robotics. They could also be downscaled and used in biomedicine applications such as drug delivery and targeted treatment.

IEEE Robotics and Automation Letters (RA-L) paper, presented at ICRA 2024, Yokohama, Japan. Cite as RA-L paper.

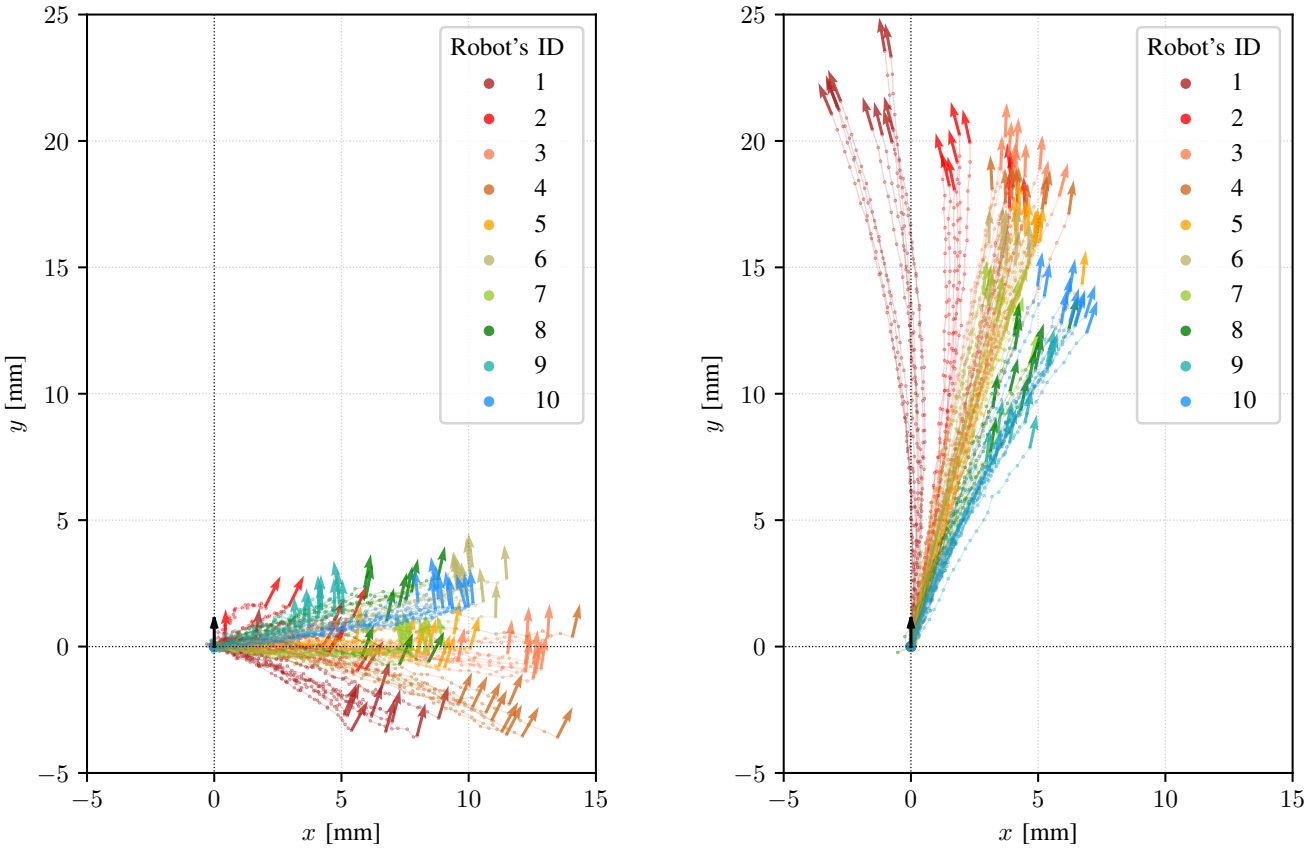

(a) Trajectories at 32 Hz show right-side locomotion. The orange-colored trajectories show insignificant rotation, the red-colored trajectories show CW rotation, and the blue and green-colored trajectories show CCW rotation.

(b) Trajectories at 52 Hz show forward locomotion. Red-colored trajectories represent almost perfect forward locomotion with lower CCW rotation and blue-colored trajectories include side locomotion components with lower CW rotation.

Fig. 5: Trajectories at two frequencies were selected from Fig. 4 to visualize the differences between the printouts of bristle-bots with different colors. Robot IDs were assigned to bristle-bots based on the results in Fig. 5b (i.e., Robot IDs do not reflect the order in which they were printed).

ACKNOWLEDGMENTS

This work was supported in part by the Czech Science Foundation (GACR) under Grant Agreement 19-26143X, in part by the Grant Agency of the Czech Technical University in Prague, grant No. SGS23/178/OHK3/3T/13. All authors thank Dr. Stephanie Krueger, who provided editorial assistance.

REFERENCES

[1] K. Zimmermann and I. Zeidis, "Worm-like locomotion as a problem of nonlinear dynamics," *Journal of Theoretical and Applied Mechanics*, vol. 45, no. 1, pp. 179–187, 2007.

[2] K. A. Daltorio, A. S. Boxerbaum, A. D. Horchler, K. M. Shaw, H. J. Chiel, and R. D. Quinn, "Efficient worm-like locomotion: slip and control of soft-bodied peristaltic robots," *Bioinspiration & biomimetics*, vol. 8, no. 3, p. 035003, 2013.

[3] R. R. Sattarov and M. A. Almaev, "Electromagnetic worm-like locomotion system for in-pipe robots: novel design of magnetic subsystem," in *IOP Conference Series: Earth and Environmental Science*, vol. 315, no. 6. IOP Publishing, 2019, p. 062013.

[4] Z. Hao, D. Kim, A. R. Mohazab, and A. Ansari, "Maneuver at micro scale: Steering by actuation frequency control in micro bristle robots," in *2020 IEEE International Conference on Robotics and Automation (ICRA)*. IEEE, 2020, pp. 10 299–10 304.

[5] D. Kim, Z. Hao, J. Ueda, and A. Ansari, "A 5 mg micro-bristle-bot fabricated by two-photon lithography," *Journal of Micromechanics and Microengineering*, vol. 29, no. 10, p. 105006, 2019.

[6] D. Kim, Z. Hao, T. H. Wang, and A. Ansari, "Magnetically-actuated micro-scale bristle-bots," in *2020 International Conference on Manipulation, Automation and Robotics at Small Scales (MARSS)*. IEEE, 2020, pp. 1–6.

[7] F. Becker, S. Boerner, V. Lysenko, I. Zeidis, and K. Zimmermann, "On the mechanics of bristle-bots-modeling, simulation and experiments," in *ISR/Robotik 2014; 41st international symposium on robotics*. VDE, 2014, pp. 1–6.

[8] E. P. Fortunić, F. Becker, K. Zimmermann, and F. Cuellar, "Bristle-bots in swarm robotics-approaches on agent development and locomotion," in *2017 IEEE International Conference on Advanced Intelligent Mechatronics (AIM)*. IEEE, 2017, pp. 1424–1429.

[9] V. Porvatov, A. Rozenblit, A. Dmitriev, O. Burmistrov, D. Petrova, G. Y. Gritsenko, E. Puhtina, E. Kretov, D. Filonov, A. Souslov *et al.*, "Optimizing self-rotating bristle-bots for active matter implementation with robotic swarms," in *Journal of Physics: Conference Series*, vol. 2086, no. 1. IOP Publishing, 2021, p. 012202.

[10] M. Jílek, K. Stránská, M. Somr, M. Kulich, J. Zeman, and L. Přeučil, "Self-stabilizing self-assembly," *IEEE Robotics and Automation Letters*, vol. 7, no. 4, pp. 9763–9769, 2022.

[11] K. Ioi, "A mobile micro-robot using centrifugal forces," in *1999 IEEE/ASME International Conference on Advanced Intelligent Mechatronics (Cat. No. 99TH8399)*. IEEE, 1999, pp. 736–741.

[12] T. Majewski, D. Szwedowicz, and M. Majewski, "Locomotion of a

IEEE Robotics and Automation Letters (RA-L) paper, presented at ICRA 2024, Yokohama, Japan. Cite as RA-L paper.

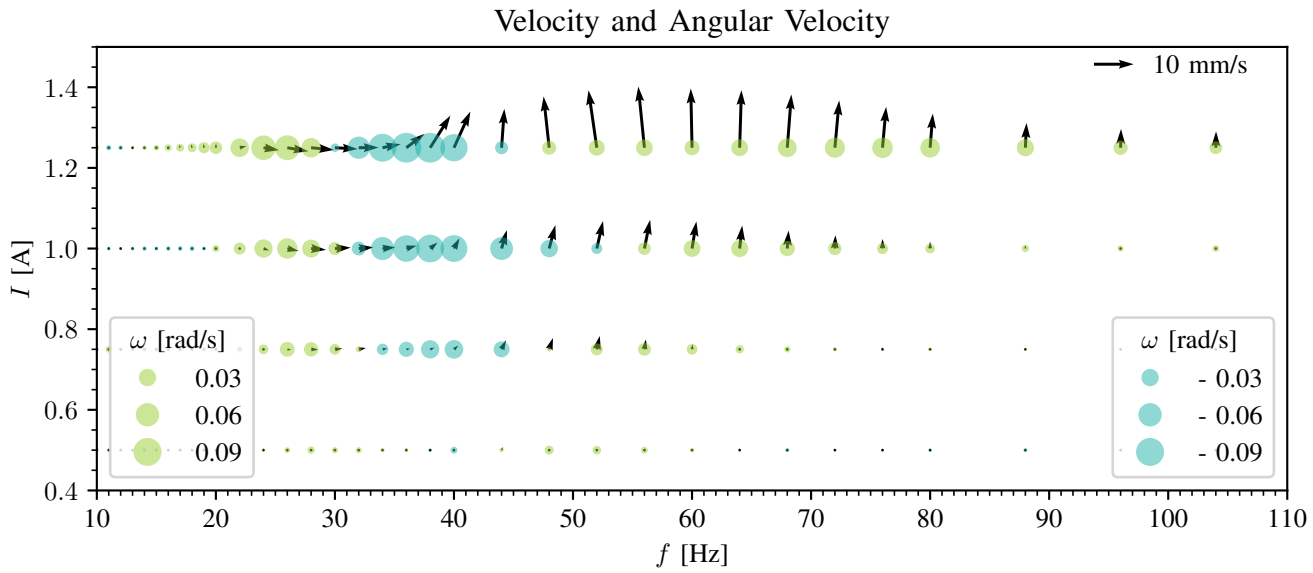

Fig. 6: This control map shows the amplitude-frequency response of bristle-bot velocities. The arrows and circles stand for translation and rotation, respectively. The color of the circles distinguishes CCW (yellow-green) and CW (blue-green) rotation. Regarding *translation*, the bristle-bots started to move right with a slight backward motion at 20 Hz. At 36 Hz, the backward component disappeared and the bristle-bots started moving forward to the right. At 50 Hz, most bristle-bots moved forward, reaching their maximum velocities (approximately 20 mm/s at 1.25 A). For higher frequencies up to 104 Hz, bristle-bot velocities decreased. Regarding *rotation*, CCW rotation was observed in the range of 20 to 30 Hz and at above 50 Hz. In the range of 30 to 50 Hz, CW rotation was observed. The relative frequency change was between 5–10% of the frequency magnitude meaning that the frequency steps gradually increased.

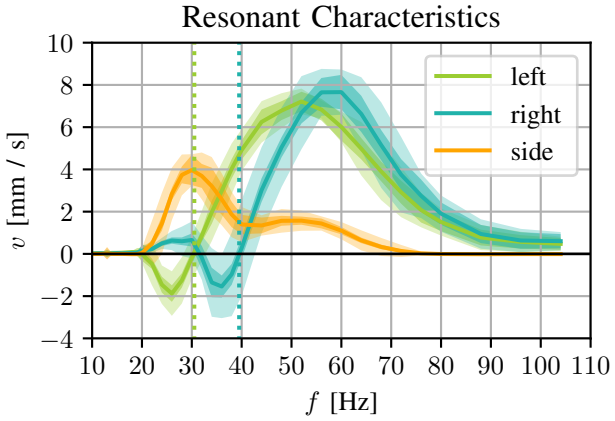

Fig. 7: Yellow-green and blue-green curves show velocities v_l and v_r for left and right legs, respectively. The orange curve shows locomotion to the right side v_s. Dispersion of the curves corresponds to printing (paler color) and measurement (richer color) errors. The natural frequencies at 30.5 and 39.5 Hz correspond to the zeros of the green curves.

mini bristle robot with inertial excitation," *Journal of Mechanisms and Robotics*, vol. 9, no. 6, p. 061008, 2017.

[13] G. Notomista, S. Mayya, A. Mazumdar, S. Hutchinson, and M. Egerstedt, "A study of a class of vibration-driven robots: Modeling, analysis, control and design of the brushbot," in *2019 IEEE/RSJ International Conference on Intelligent Robots and Systems (IROS)*. IEEE, 2019, pp. 5101–5106.

[14] D. Kim, Z. Hao, A. R. Mohazab, and A. Ansari, "On the forward and backward motion of milli-bristlebots," *International Journal of Non-Linear Mechanics*, vol. 127, p. 103551, 2020.

[15] G. Cicconofri and A. DeSimone, "Motility of a model bristle-bot: A theoretical analysis," *International Journal of Non-Linear Mechanics*, vol. 76, pp. 233–239, 2015.

[16] G. Cicconofri, F. Becker, G. Noselli, A. Desimone, and K. Zimmermann, "The inversion of motion of bristle bots: analytical and experimental analysis," in *ROMANSY 21-Robot Design, Dynamics and Control: Proceedings of the 21st CISM-IFToMM Symposium, June 20-23, Udine, Italy*. Springer, 2016, pp. 225–232.

[17] Z. Faraji Rad, P. D. Prewett, and G. J. Davies, "High-resolution two-photon polymerization: The most versatile technique for the fabrication of microneedle arrays," *Microsystems & nanoengineering*, vol. 7, no. 1, p. 71, 2021.

[18] V. Reichel, A. Kovács, M. Kumari, É. Bereczk-Tompa, E. Schneck, P. Diehle, M. Pósfai, A. M. Hirt, M. Duchamp, R. E. Dunin-Borkowski *et al.*, "Single crystalline superstructured stable single domain magnetite nanoparticles," *Scientific reports*, vol. 7, no. 1, p. 45484, 2017.

[19] E. Dennison, "On-axis field of an ideal helmholtz coil," 2014, https://web.archive.org/web/20140327080853/http://www.netdenizen.com/emagnet/helmholtz/idealhelmholtz.htm [Accessed: 14.8.2023].

[20] E. Bronaugh, "Helmholtz coils for calibration of probes and sensors: limits of magnetic field accuracy and uniformity," in *Proceedings of International Symposium on Electromagnetic Compatibility*, 1995, pp. 72–76.

[21] R. P. Feynman, R. B. Leighton, and M. Sands, *The Feynman Lectures on Physics. Volume 2: Mainly Electromagnetism and Matter. 6th printing*. Addison-Wesley, Reading MA u. a, 1977.

[22] H. Goldstein, C. Poole, and J. Safko, "Classical mechanics," 2002.

[23] T. A. R. Laboratory, "Apriltag," 2010, https://april.eecs.umich.edu/software/apriltag [Accessed: 14.8.2023].